European Journal of Radiology 116 (2019) 212–218

Contents lists available at ScienceDirect

European Journal of Radiology

journal homepage: www.elsevier.com/locate/ejrad

Research article

Using texture analysis of head CT images to differentiate osteoporosis from normal bone density

Yusuke Kawashima[a,d], Akifumi Fujita[a,e], Karen Buch[a], Baojun Li[a], Muhammad M. Qureshi[a,b], Margaret N. Chapman[a], Osamu Sakai[a,b,c,*]

[a] Department of Radiology, Boston Medical Center, Boston University School of Medicine, Boston Massachusetts, United States
[b] Department of Radiation Oncology, Boston Medical Center, Boston University School of Medicine, Massachusetts, United States
[c] Department of Otolaryngology – Head and Neck Surgery, Boston Medical Center, Boston University School of Medicine, Boston Massachusetts, United States
[d] Department of Radiology, Nihon University School of Dentistry at Matsudo, Chiba, Japan
[e] Department of Radiology, Jichi Medical University School of Medicine, Shimotsuke, Tochigi, Japan

ARTICLE INFO

Keywords:
CT
Craniofacial bones
Texture analysis
Osteoporosis
Normal bone density

ABSTRACT

Objectives: To investigate the use of texture analysis for the detection of osteoporosis on noncontrast head CTs, and to explore optimal sampling regions within the craniofacial bones.

Methods: In this IRB-approved, retrospective study, the clivus, bilateral sphenoid triangles and mandibular condyles were manually segmented on each noncontrast head CT, and 41 textures features were extracted from 29 patients with normal bone density (NBD); and 29 patients with osteoporosis. Basic descriptive statistics including a false discovery rate correction were performed to evaluate for differences in texture features between the cohorts.

Resuls: Sixteen texture features demonstrated significant differences ($P < 0.01$) between NBD and osteoporosis in the clivus including 4 histogram features, 2 gray-level co-occurrence matrix features, 8 gray-level run-length features and 2 Law's features. Nineteen texture features including 9 histogram features, 1 GLCM features, 2 GLRL features, 5 Law's features and 2 GLGM features demonstrated statistically significant differences in both sides of the sphenoid triangles. A total 24 texture features demonstrated statistically significant differences between normal BMD and osteoporosis in the left sphenoid and a total of 31 texture features in the left condyle. Furthermore, a total of 22 texture features including 6 histogram features, 3 GLCM features, 9 GLRL features, 2 Law's features and 2 GLGM features demonstrated statistically significant differences in both sides of the mandibular condyles.

Conclusion: The results of this investigation suggest that specific texture analysis features derived from regions of interest placed within multiple sites within the skull base and maxillofacial bones can distinguish between patients with normal bone mineral density compared to those with osteoporosis. This study demonstrates the potential utility of a texture analysis for identification of osteoporosis on head CT, which may help identify patients who have not undergone screening with traditional DXA.

1. Introduction

Osteoporosis is a diffuse osseous disease characterized by decreases in both cancellous and cortical bone mass as well as microarchitectural deterioration of bone, ultimately leading to an increased risk of fracture [1,2]. The prevalence of osteoporosis across the population is expected to increase with increasing life expectancy [3]. The early detection of osteoporosis is clinically important for the management, treatment, and

Abbreviations: NPC, nasopharyngeal carcinoma; ^{18}F-FDG, PET [18F]-fluorodeoxyglucose positron emission tomography; CT, computed tomography; IQR, interquartile range; GLCM, gray-level co-occurrence matrix; GLRL, gray-level run length; SRLGE, short-run low gray-level emphasis; SRHGE, short-run high gray-level emphasis; GLGM, gray-level gradient matrix; SRE, short-run emphasis; LRE, long-run emphasis; GLN, gray-level nonuniformity; RLN, run-length nonuniformity; RP, run percentage; LGRE, low gray-level run emphasis; HGRE, high gray-level run emphasis; SRLGE, short-run low gray-level emphasis; SRHGE, short-run high gray-level emphasis; LRLGE, long-run low gray-level emphasis; LRHGE, long-run high gray-level emphasis; MGR, mean gradients; VGR, variance of gradients

* Corresponding author at: Department of Radiology, Boston Medical Center, Boston University School of Medicine, FGH Building, 3rd Floor, 820 Harrison Avenue, Boston, Massachusetts 02118, United States.
E-mail address: osamu.sakai@bmc.org (O. Sakai).

https://doi.org/10.1016/j.ejrad.2019.05.009
Received 8 January 2019; Received in revised form 1 April 2019; Accepted 7 May 2019

risk stratification of patients to ultimately decrease the prevalence of osteoporotic fracture and ensuing morbidity [4].

Osteoporosis is reported to affect approximately 9.9 million Americans [5]. The United States Preventive Services Task Force (USPSTF) recommends screening for osteoporosis in women aged 65 and above, and in younger women with risk factors for fractures equal to those of a 65-year-old female [6]. About one out of every two Caucasian women will experience an osteoporosis-related fracture at some point in her lifetime, as well as approximately one in five men [2]. Several studies have demonstrated that there is a large population of women at risk for osteoporotic fractures who have not undergone the recommended screening for osteoporosis. The failure to undergo these screening tests may be related to lack of access to these screening tests and routine medical care, as well as decreased awareness of osteoporosis fracture risk and associated morbidity [7–9].

Quantitative measures of bone mass serve as important diagnostic indicators for the determination of fracture risk and for prognostication in patients undergoing therapy for osteoporosis [10]. The most widely used method of assessing bone mass is bone mineral densitometry (BMD) which uses dual energy X-ray absorptiometry (DXA) [1,11], a method that has been shown to be a good predictor of fracture risk in patients with osteoporosis [1]. BMD alone may be insufficient to determine the strength of both the cancellous bone and trabecular bone architecture, two features which are both known to be important for the determination of overall bone strength [6]. Several imaging modalities, such as multidetector-row CT, quantitative CT, quantitative ultrasound (US) and MRI have been used for the assessment of bone quality, in addition to BMD for the prediction of bone strength [10,12,13]. Since there is a large population of women who do not undergo routine screening for osteoporosis, the investigation into other imaging modalities, which may be more prevalent and easier to access in the community is important. Moreover, the possibility of using alternative imaging modalities (CT and MRI), and previously obtained examinations, which may have been obtained for unrelated clinical purposes, to evaluate these patients for osteoporosis would be of clinical and epidemiologic interest [7–9]. This would ultimately serve to decrease the number of patients who have not had an assessment of BMD and may help to expediate treatment and management of osteoporosis in these patients.

The use of mathematical algorithms to evaluate the inherent texture within an image is becoming increasingly used within the field of radiology. Image texture is defined as a complex visual pattern within an image that consists of simpler sub-patterns with characteristic features that may be evaluated through quantitative analysis [14,15]. Texture analysis has been previously applied to imaging of other areas of the body such as the liver, brain, cartilage, and of tumors [15–21]. Despite the increasing use of texture analysis in radiology research, there are few studies utilizing texture analysis applied to CT images for the differentiation of normal bone density from osteoporosis. The purpose of this study was to investigate the utility of a texture analysis applied to noncontrast head CT examinations for the detection of osteoporosis, and to explore the best anatomic region to use for the evaluation of trabecular architecture in the craniofacial bones.

2. Materials and methods

2.1. Patients

Following IRB approval, an electronic search was performed through the Radiological Information System (RIS) to identify patients who underwent both noncontrast head CT and DXA scans within 12 months of each other. All patients included in this study had noncontrast head CT scans performed between January 2009 and June 2015. The DXA scans were reviewed by a radiologist for the determination of BMD. Patients with a diagnosis of osteoporosis identified on DXA as well as and age and gender-matched control patients with normal bone density identified on DXA were included in this study. Patients with a history of malignancy, hematological disorder, prior infection or focal osseous lesions in the region-of-interest (ROI) were excluded from this study.

2.2. Normal bone density vs osteoporosis

BMD measurements were performed by placing an ROI within the lumber spine and in the femoral neck performed on the DXA devices [1]. For this study, we referred to the WHO diagnostic classification of normal BMD that was defined as a BMD within 1 standard deviation (SD) of a “young normal” adult [22]. Using the same WHO classification, osteoporosis is defined as a BMD 2.5 SD or more below that of a “young normal” adult [22]. We defined “normal bone density” as patients with normal bone density in both the femoral neck and lumbar spine according to the T score which was larger than -1 SD. “Osteoporosis” was defined as patients with osteoporosis in both femoral neck and lumbar spine according to the T-score which was smaller than -2.5 SD. Patients with abnormal BMD meeting the WHO classification for osteoporosis in both sampled regions of the lumbar spine and femoral head were included in this study [22].

2.3. CT imaging protocol

Noncontrast head CT scans were axially acquired on 64-detector row CT scanners (Lightspeed VCT; GE Healthcare, Milwaukee, Wisconsin) with 120 kV, 225 mA and 1 s/rotation, and Adaptive Statistic Iterative Reconstruction was set at 10% dose reduction. Five and 1.25 mm thick images were reconstructed using soft tissue and bone reconstruction kernels per our institutional clinical protocol. Axial 1.25 mm images in bone kernel reconstruction with 0.4 mm x 0.4 mm in-plane resolution were used for this analysis. The quality of the scans was evaluated by a radiologist, and any scans with motion artifact were eliminated from the study.

2.4. Image segmentation and texture analysis

Manual segmentation was performed on five osseous, craniofacial regions including the clivus, bilateral sphenoid triangles (greater wing of sphenoid), and the bilateral mandibular condyles. This segmentation was performed on a dedicated AW workstation version 4.4 (GE Healthcare, Milwaukee, Wisconsin). Triangular or ovoid shaped regions-of-interest were manually places in each region including only the cancellous bone and excluding the cortical bone (Fig. 1). These contours were performed on three consecutive axial images. The segmented contours were then imported into in-house developed texture analysis software, and texture features were calculated for each of the five regions.

A total of 41 texture features were calculated using an in-house developed texture analysis program which includes 13 histogram features, 5 gray level co-occurrence matrix (GLCM) features, 11 gray level run-length (GLRL) features, 4 gray level gradient matrix (GLGM) features, and 9 Laws features. All texture features were calculated on each contoured image slice. Texture features extracted from each image slice, within an image, for a given contoured osseous structures were averaged, a methodology previously used and described in the literature [15,21].

GLCM features, in contrast to histogram features, are spatially dependent. The GLCM is symmetric with rows and columns ranging from 0 to Ng, where Ng equals the number of gray levels in the image. Such notation allows GLCM elements in row i and column j to represent the frequency in which a given gray level of value i is horizontally adjacent to gray level j. Calculations in the horizontal, 45°, vertical, and 135° directions were averaged together to minimize directional dependence within the liver samples. GLCM features used in our analysis, proposed by Haralick et al. and previously documented in the literature [13,23].

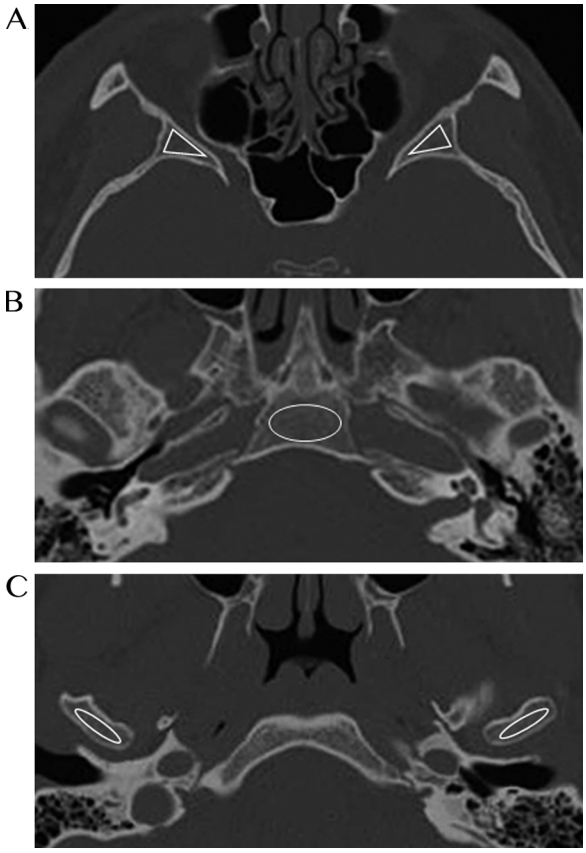

Fig. 1. Example of regions-of-interest (ROIs) placement. Triangular (A) or oval shaped (B and C) ROIs were manually placed to include only the cancellous bone excluding the cortical bone. A, Sphenoid triangles (greater wing of sphenoid) (*triangles*). B, Clivus (*oval*). C, Mandibular condyles (*ovals*). This was performed in the three consecutive axial images for each region.

GLRL matrix features are similar to GLCM features as they are also spatially dependent. The GLRL matrix is quantized to Ng gray levels to simplify texture extraction. Row index i of the matrix represents gray level while column index j represents the run-length of j, defined as the number of adjacent pixels of equal gray value in a given direction. Elements within the matrix represent the frequency of pixel line segments, also known as runs, with run-length j and a gray level i. The same directions that were considered for GLCM features were also averaged for the GLRL matrix. Features that were included in the analysis included short run emphasis (SRE), long run emphasis (LRE), gray-level non-uniformity (GLN), run-length non-uniformity (RLN), run percentage (RP), low gray-level run emphasis (LGRE), high gray-level run emphasis (HGRE), short run low gray-level emphasis (SRLGE), short run high gray-level emphasis (SRHGE), long run low gray-level emphasis (LRLGE), and long run high gray-level emphasis (LRHGE), and were previously described in the literature [13].

GLGM features were employed to provide a histogram of the absolute gradient values in the liver segment [13]. As a preprocessing step, gradients of every pixel within the liver segment were computed using a 3 × 3 neighborhood. GLGM features that were used to summarize the gradient values of pixels include the mean, variance, skewness and kurtosis.

The final category of the extracted texture feature investigated in this study are the Laws' features, which are based on unidimensional vectors described by Laws [24]. Vectors described by Laws included level, spot, edge, ripple, wave, undulation and oscillation [25,26]. The vectors level, edge, ripple and spot were used for our analysis. Two 5-pixel vectors are multiplied to create two-dimensional filter masks, which were applied across an image. Laws' features that were included in the analysis included L1, L2, L3, L4, L5, L6, L7, L8 and L9.

2.5. Statistical analysis

A total of 41 textures features were compared between patients with normal bone density and patients with osteoporosis using a student's *t*-test for independent samples. To adjust for multiple comparisons, a false discovery rate (FDR) correction was performed and the FDR corrected *P*-values (term *Q*-values) were calculated in addition to raw *P*-values using the Benjamini and Hochberg method described in the literature [27]. Statistical computations were performed using SAS 9.3 software (SAS Institute, Cary, NC). The PROC MULTTEST function in SAS was used to calculate the *Q*-values. A two-tailed *P*-value of < 0.05 was used to evaluate statistical significance.

3. Results

3.1. Patient characteristics

The patient cohort was comprised of a total of 58 patients (6 males and 52 females, age ranged from 51 to 88 years, mean age 68.3, standard division of 9.0 years); 29 patients with osteoporosis (3 males, 26 females, age range; 52–88 years, mean age; 68.1, standard division of 9.3) and 29 age- and gender-matched control patients with normal bone density (3 males, 26 females, ranging in age from 51 to 88 years (mean age of 68.8 years, standard division of 8.7 years).

3.2. Texture analysis

A total of 16 texture features demonstrated a statistically significant difference between normal BMD and osteoporosis for the contoured clival segments including four histogram features, two GLCM features, eight GLRL features and two Law's features. A total of 26 texture features demonstrated a statistically significant difference between normal BMD and osteoporosis in the right sphenoid triangle and a total of 21 texture features in the left sphenoid triangle. Furthermore, 19 texture features including nine histogram features, one GLCM features, two GLRL features, five Law's features and two GLGM features demonstrated a statistically significant difference in both sides of the sphenoid triangle. A total 24 texture features demonstrated a statistically significant difference between normal BMD and osteoporosis in the left sphenoid and a total of 31 texture features in the left condyle. Furthermore, a total of 22 texture features including six histogram features, three GLCM features, nine GLRL features, two Law's features and two GLGM features demonstrated a statistically significant difference in both sides of the condyle. Tables 1, 2 and 3 demonstrates texture parameters differentiating between normal BMD and osteoporosis patients in the clivus, both sides of the sphenoid triangle, and both sides of the mandibular condyle.

Mean, median, 2d std, range and geo mean (categorized as histogram features), homogeneity (categorized as GLCM features), HGRE (categorized as GLRL features) and L1, L2, L4 and L9 (categorized as Law's features) showed statistically significant differences in all regions. After the FDR correction, mean and median (categorized as histogram features) remained statistically significant difference in all regions. GLRL features showed numerous statistically significant texture features between normal BMD and osteoporosis compared to other texture features.

4. Discussion

The results of this study demonstrated statistically significant differences in texture analysis features between patients with osteoporosis compared to age- and gender-matched control patients with normal BMD. Multiple anatomic regions within the osseous skull-base and mandible were sampled with similar texture feature patterns

Table 1
Texture parameters differentiating between normal bone density and osteoporosis patients in the clivus.

	Normal bone density (N = 29)		Osteoporosis (N = 29)			
	Mean	SD	Mean	SD	*P*-value	*Q*-value
Histogram						
Mean	1161.95	112.47	1030.99	79.81	< 0.0001	< 0.0001
Median	1194.64	105.22	1076.69	74.55	< 0.0001	< 0.0001
STD	356.92	44.77	345.82	55.45	0.148	0.173
Range	192.12	123.07	154.23	119.49	0.041	0.072
Geometric mean	925.11	133.68	796.73	125.15	< 0.0001	< 0.0001
Harmonic mean	297.29	184.60	242.73	146.75	0.032	0.064
2nd STD	66.53	42.12	53.94	41.54	0.049	0.076
STD5	83.26	47.89	69.20	46.70	0.052	0.076
STD9	97.67	47.00	85.23	47.58	0.085	0.115
4th moment	8.76e10	3.32e10	7.06e10	4.81e10	0.007	0.026
IQR	247.65	62.93	264.32	132.23	0.290	0.305
Entropy	6.91	0.19	6.93	0.27	0.593	0.607
GLCM						
Entropy	1.40	0.36	1.24	0.40	0.008	0.026
Contrast	27.12	23.32	22.47	26.15	0.217	0.234
Correlation	0.80	0.17	0.85	0.17	0.046	0.075
Energy	0.02	0.01	0.02	0.02	0.016	0.046
Homogeneity	0.55	0.17	0.60	0.19	0.046	0.075
GLRL						
SRE	0.03	0.01	0.04	0.02	< 0.0001	< 0.0001
LRE	0.03	0.02	0.05	0.02	< 0.0001	< 0.0001
GLN	0.03	0.02	0.05	0.02	< 0.0001	< 0.0001

	Normal bone density (N = 29)		Osteoporosis (N = 29)			
	Mean	SD	Mean	SD	*P*-value	*Q*-value
GLRL, continued						
RLN	0.03	0.02	0.05	0.02	< 0.0001	< 0.0001
RP	353.75	48.94	320.88	62.08	0.0001	0.0004
LGRE	342.18	52.64	307.28	65.71	0.0002	0.001
HGRE	335.57	54.89	295.40	72.07	< 0.0001	< 0.0001
SRLGE	343.55	51.65	307.22	65.47	< 0.0001	< 0.0001
SRHGE	1832.80	1505.42	2172.66	1522.36	0.141	0.169
LRLGE	3930.17	4079.41	5067.71	4273.21	0.074	0.104
LRHGE	2634.59	2647.74	3651.95	3157.52	0.023	0.053
Law's features						
L1	8.70e5	6.13e5	6.70e5	6.45e5	0.038	0.069
L2	2.19e5	1.85e5	1.58e5	1.82e5	0.032	0.064
L3	6.85e4	6.52e4	4.63e4	5.67e4	0.018	0.047
L4	3.33e5	2.77e5	2.44e5	2.71e5	0.034	0.064
L5	4.55e4	4.47e4	3.09e4	3.82e4	0.021	0.053
L6	1.81e4	1.72e4	1.31e4	1.60e4	0.053	0.076
L7	2.80e4	2.77e4	1.93e4	2.44e4	0.029	0.064
L8	1.28e4	9683.46	1.07e4	1.03e4	0.159	0.181
L9	1.64e5	1.44e5	1.13e5	1.30e5	0.016	0.046
GLGM						
MGR	8.75	9.63	11.09	10.66	0.131	0.166
VGR	8033.49	2557.41	1.74e4	5.77e4	0.134	0.166
Skewness	29.91	17.72	25.11	19.20	0.089	0.117
Kurtosis	1345.41	1140.55	1098.57	1304.98	0.186	0.205

Abbreviations: N, number of patients; STD, standard deviation; IQR, interquartile range; GLCM, gray level co-occurrence matrix; GLRL, gray level run length; SRE, short-run emphasis; LRE, long-run emphasis; GLN, gray-level nonuniformity; RLN, run-length, nonuniformity; RP, run percentage; LGRE, low gray-level run emphasis; HGRE, high gray-level run emphasis; SRLGE, short-run low gray-level emphasis; SRHGE, short-run high gray-level emphasis; LRLGE, long-run low gray-level emphasis; LRHGE, long-run high gray-level emphasis; MGR, mean gradients; VGR, variance gradients.
Note: For all analyses 29 patients contributed 87 measurements.

discriminating between these two patient groups.

The use of texture analysis, which is a non-invasive, quantitative, post-processing imaging analysis method, to evaluate BMD in the skull base and mandible on noncontrast CT has not been previously described. Similar studies have employed the use of texture analysis applied elsewhere in the body [1,15,16,18,20,21]. Previously, Ouyang et al. [1] assessed the vertebral trabecular bone structure using texture analysis and established not only interrelationships among biomechanical, densitometric, and textural measures from radiographic trabecular bone patterns, but also demonstrated concurrence of these measures on anatomic orientation. Kavitha et al. [11] used texture features applied to the mandibular cortical width derived from digital panoramic radiographs to be a useful marker for the assessment of osteoporosis. Ito et al. [28] also utilized texture analysis applied to the spine to evaluate fracture risk in elderly women. Castellanos et al. [29] assessed the L3 vertebral on CT images using texture analysis concluded that texture analysis could help to determine osteoporosis. Lespessailles et al. [30] used texture analysis to the X-ray of the calcaneus; found that the combination of BMD and the texture analysis provides a better assessment of the fracture risk than that obtainable solely by BMD measurement. In our study, several texture features demonstrated statistically significant differences between patients with normal bone mineral

Table 2
Texture parameters differentiating between normal bone density and osteoporosis patients in the right and left sphenoid.

	Right sphenoid						Left sphenoid					
	Normal bone density (N = 29)		Osteoporosis (N = 29)				Normal bone density (N = 29)		Osteoporosis (N = 29)			
	Mean	SD	Mean	SD	*P*-value	*Q*-value	Mean	SD	Mean	SD	*P*-value	*Q*-value
Histogram												
Mean	1095.55	180.63	972.85	147.91	< 0.0001	< 0.0001	1107.12	277.2	970.19	128.6	< 0.0001	< 0.0001
Median	1254.81	184.95	1101.09	145.76	< 0.0001	< 0.0001	1239.56	332.22	1105.93	116.44	0.001	0.002
STD	533.1	75.89	484.73	186.26	0.027	0.043	551.97	160.16	475.11	210.97	0.007	0.017
Range	376.6	224.23	242.39	218.88	< 0.0001	< 0.0001	375.36	213.11	219.25	187.63	< 0.0001	< 0.0001
Geometric mean	714.74	195.84	649.79	192.43	0.029	0.045	745.47	258.14	646.25	170.34	0.003	0.008
Harmonic mean	157.71	113.65	162.15	133.43	0.813	0.813	185.06	149.83	154.2	122.22	0.138	0.203
2nd STD	134.06	78.67	86.31	77.68	< 0.0001	< 0.0001	133.24	74.72	77.68	65.8	< 0.0001	< 0.0001
STD5	159.03	78.39	104.45	77.81	< 0.0001	< 0.0001	158.99	75.64	94.95	65.3	< 0.0001	< 0.0001
STD9	186.94	80.08	120.48	66.74	< 0.0001	< 0.0001	182.1	75.78	115.22	61.39	< 0.0001	< 0.0001
4th moment	1.93E+11	1.03E+11	3.26E+12	1.45E+13	0.052	0.068	2.43E+12	1.19E+13	3.44E+12	1.79E+13	0.663	0.714
IQR	844.97	257.53	637.62	285.92	< 0.0001	< 0.0001	773.81	267.65	607.48	266.12	< 0.0001	< 0.0001
Entropy	7.21	0.28	7.04	0.52	0.007	0.018	6.98	0.55	7.1	0.45	0.138	0.208
GLCM												
Entropy	1.25	0.42	1.16	0.46	0.185	0.195	1.19	0.41	1.14	0.39	0.479	0.559
Contrast	52.38	47.69	38.97	53.83	0.084	0.09	51.43	45.28	35.84	48.22	0.029	0.052
Correlation	0.8	0.18	0.86	0.18	0.055	0.071	0.81	0.17	0.86	0.18	0.049	0.083
Energy	0.01	0.01	0.03	0.04	0.001	0.004	0.02	0.03	0.02	0.03	0.662	0.714
Homogeneity	0.47	0.16	0.57	0.2	0.0001	0.001	0.48	0.18	0.58	0.19	0.0005	0.002
GLRL												
SRE	0.06	0.02	0.07	0.03	0.081	0.09	0.07	0.06	0.06	0.03	0.397	0.491
LRE	0.06	0.02	0.07	0.04	0.024	0.04	0.07	0.06	0.07	0.04	0.79	0.83
GLN	0.06	0.02	0.07	0.06	0.061	0.074	0.07	0.04	0.07	0.04	0.951	0.951
GLRL, continued												
RLN	0.06	0.02	0.07	0.04	0.046	0.065	0.07	0.06	0.07	0.04	0.863	0.884
RP	301.34	42.89	283.96	55.35	0.022	0.038	296.4	62.44	287.74	54.33	0.33	0.421
LGRE	301.52	42.96	280.68	58.36	0.008	0.018	297.56	63.5	287.37	59.37	0.276	0.365
HGRE	295.85	41.12	269.53	76.31	0.005	0.014	298.4	70.82	274.37	72.66	0.028	0.052
SRLGE	303.25	41.45	284.4	57.56	0.014	0.027	296.4	63.44	286.2	60.16	0.278	0.365
SRHGE	1284.61	1613.09	2023.51	1831.26	0.005	0.014	1245.18	1447.28	2035.23	1759.89	0.001	0.004
LRLGE	2728.14	3746.08	3965.93	3858.48	0.033	0.05	1972.28	2512.63	4001.09	3845.81	< 0.0001	< 0.0001
LRHGE	1726.95	2218.05	2658.77	2596.52	0.012	0.024	1354.92	1742.76	2874.6	2759.6	< 0.0001	< 0.0001
Law's feature*												
L1	1.12E+06	9.21E+05	5.96E+05	6.39E+05	0.0003	0.001	1.24E+06	8.98E+05	6.35E+05	6.83E+05	< 0.0001	< 0.0001
L2	1.98E+05	2.36E+05	1.05E+05	1.55E+05	0.009	0.019	2.41E+05	2.49E+05	1.23E+05	1.70E+05	0.001	0.004
L3	5.10E+04	7.02E+04	2.62E+04	4.48E+04	0.018	0.033	6.31E+04	7.11E+04	3.28E+04	5.34E+04	0.005	0.011
L4	3.28E+05	3.36E+05	1.74E+05	2.27E+05	0.003	0.008	3.96E+05	3.51E+05	1.96E+05	2.49E+05	0.0002	0.001
L5	3.29E+04	4.82E+04	1.77E+04	3.16E+04	0.035	0.051	4.07E+04	5.02E+04	2.34E+04	3.97E+04	0.025	0.05
L6	1.48E+04	2.50E+04	7969.78	1.52E+04	0.065	0.076	1.62E+04	2.17E+04	1.02E+04	1.82E+04	0.078	0.126
L7	1.96E+04	3.23E+04	1.03E+04	2.03E+04	0.052	0.068	2.36E+04	3.08E+04	1.33E+04	2.41E+04	0.03	0.052
L8	1.37E+04	1.99E+04	8548.21	1.18E+04	0.074	0.084	1.36E+04	1.61E+04	1.00E+04	1.36E+04	0.148	0.214
L9	1.50E+05	1.65E+05	7.49E+04	1.06E+05	0.003	0.008	1.78E+05	1.66E+05	8.79E+04	1.23E+05	0.0003	0.001
GLGM												
MGR	4.44	5.07	10.33	19.71	0.008	0.018	6.71	13.82	10.83	25.76	0.192	0.268
VGR	5147.37	2223.03	1.24E+05	5.81E+05	0.059	0.073	7.78E+04	3.83E+05	1.48E+05	7.66E+05	0.443	0.532
Skewness	43.73	26.38	30.37	24.71	0.001	0.003	43.93	25.25	31.31	26.55	0.002	0.004
Kurtosis	2802.69	2486.17	1633.98	2093.09	0.001	0.004	2773.3	2487.8	1798.85	2352.68	0.009	0.018

* In right sphenoid analysis, 24 and 26 patients contributed 62 and 73 measurements to normal bone density and osteoporosis groups, respectively. In left sphenoid analysis, 25 and 28 patients contributed 68 and 76 measurements to normal bone density and osteoporosis groups, respectively. For all other analyses 29 patients contributed 87 measurements.

density and osteoporosis based on region-of-interest sampling at multiple points within the craniofacial bones. Among the investigated regions, both sides of the mandibular condyle demonstrated a statistically significant difference in discriminating between patient groups. While these texture features may reflect some inherent changes related to superimposed osteoarthritis within the temporomandibular joints, the results of this study demonstrate the ability of a texture analysis to distinguish between osteoporosis and normal bone mineral density, despite potential osteoarthritic changes. Both the left and right sphenoid triangles demonstrated a statistically significant difference between the normal bone mineral density and osteoporotic patient cohorts, but in a fewer number of texture analysis features compared to the number of texture analysis features extracted from the mandibular condyles. This may potentially be related to different or more pronounced architectural changes within the mandibular condyles compared to the sphenoid triangles. Significant differences between the patients with a normal bone mineral density and osteoporosis were seen in the texture analysis features extracted from the clivus. The clivus is a much large structure, resistant to osteoarthritis changes, and may therefore be easier to interrogate compared to the small sphenoid triangles and mandibular condyles, which may be affected by osteoarthritic changes.

With specific regard to the texture features investigated in this study, there were two texture features, mean and median, that demonstrated statistically significant differences in all regions. We believe these texture features are reflective of osteoporotic changes in the cancellous bone. According to the prior study, RLN is lower in osteoporosis with fracture cases than normal bone density on the L3 vertebra

Table 3
Texture parameters differentiating between normal bone density and osteoporosis patients in in the right and left condyles.

	Right condyle						Left condyle					
	Normal bone density (N = 29)		Osteoporosis (N = 29)				Normal bone density (N = 29)		Osteoporosis (N = 29)			
	Mean	SD	Mean	SD	*P*-value	*Q*-value	Mean	SD	Mean	SD	*P*-value	*Q*-value
Histogram												
Mean	1090.22	127.21	992.08	82.68	< 0.0001	0.0001	1098.63	145.25	962.09	187.73	< 0.0001	0.0001
Median	1220.43	126.91	1100.39	62.41	< 0.0001	0.0001	1231.05	147.19	1108.37	74.47	< 0.0001	0.0001
STD	475.13	67.47	470.76	259.21	0.879	0.879	486.67	82.31	490.36	227.13	0.887	0.887
Range	286.34	169.22	207.52	206.49	0.007	0.018	308.4	187.91	224.52	203.84	0.005	0.01
Geometric mean	747.23	170.96	696.85	134.15	0.032	0.052	752.93	176.41	681.75	140.93	0.004	0.008
Harmonic mean	177.74	127.39	171.62	107.31	0.732	0.75	176.18	120.09	164.68	116.73	0.523	0.536
2nd STD	101.03	59.04	73.5	73.35	0.007	0.018	108.29	65.27	79.2	71.89	0.006	0.011
STD5	119.08	61.35	90.31	79.15	0.008	0.019	127.09	69.37	95.22	76.09	0.004	0.009
STD9	142.26	65.37	98.44	57.44	< 0.0001	0.0001	149.45	74.42	118.88	87.26	0.014	0.02
4th moment	1.40E + 11	4.87E + 10	5.28E + 12	2.29E + 13	0.039	0.06	5.91E + 11	3.67E + 12	5.45E + 12	1.83E + 13	0.017	0.023
IQR	583.82	296.92	435.89	224.9	0.0003	0.003	592.75	268.32	518.68	268.12	0.07	0.084
Entropy	7.08	0.33	6.92	0.64	0.042	0.061	7.04	0.43	6.88	0.69	0.066	0.081
GLCM												
Entropy	1.32	0.38	1.13	0.46	0.004	0.015	1.28	0.42	1.06	0.45	0.001	0.005
Contrast	43.36	39.25	32.76	43.23	0.092	0.119	45.64	40.21	35.1	44.19	0.102	0.115
Correlation	0.81	0.17	0.83	0.19	0.362	0.39	0.8	0.17	0.85	0.18	0.043	0.057
Energy	0.01	0.01	0.03	0.06	0.002	0.011	0.02	0.03	0.04	0.06	0.011	0.016
Homogeneity	0.51	0.16	0.6	0.21	0.002	0.011	0.5	0.18	0.6	0.22	0.002	0.006
GLRL												
SRE	0.05	0.02	0.06	0.04	0.017	0.033	0.05	0.03	0.07	0.06	0.008	0.013
LRE	0.06	0.02	0.07	0.05	0.007	0.018	0.05	0.03	0.08	0.07	0.002	0.006
GLN	0.06	0.02	0.07	0.07	0.012	0.026	0.06	0.04	0.09	0.07	0.006	0.011
GLRL, continued												
RLN	0.05	0.02	0.07	0.05	0.004	0.015	0.06	0.04	0.09	0.07	0.003	0.007
RP	322.08	58.97	295.05	70.46	0.007	0.018	319.36	64.39	288.21	60.5	0.001	0.005
LGRE	311.21	57.07	278.17	77.7	0.002	0.01	318.67	65.74	279.3	72.1	0.0002	0.002
HGRE	302.69	51.93	261.33	95.77	0.001	0.005	302.28	71.35	251.66	98.47	0.0002	0.002
SRLGE	320.17	52.12	289.4	71.44	0.001	0.01	310.94	68.45	271.74	73.74	0.0004	0.002
SRHGE	1573.4	1731.16	1916.08	1618.13	0.179	0.215	1405.39	1438.06	1768.96	1591.29	0.116	0.128
LRLGE	3368.42	4056.46	4634.58	4445	0.051	0.072	2337.82	2781.46	3606.9	3829.88	0.013	0.02
LRHGE	2080.42	2343.5	3063.17	2971.19	0.017	0.033	2284.23	2998.2	2908.14	3171.87	0.184	0.198
Law's features*												
L1	1.03E + 06	8.32E + 05	6.74E + 05	7.37E + 05	0.006	0.018	1.09E + 06	9.00E + 05	5.39E + 05	6.10E + 05	< 0.0001	0.0001
L2	2.20E + 05	2.39E + 05	1.40E + 05	1.95E + 05	0.027	0.047	2.36E + 05	2.56E + 05	1.03E + 05	1.52E + 05	0.0004	0.002
L3	5.73E + 04	6.63E + 04	4.07E + 04	5.80E + 04	0.107	0.133	6.42E + 04	7.52E + 04	2.79E + 04	4.64E + 04	0.001	0.004
L4	3.36E + 05	3.32E + 05	2.26E + 05	2.84E + 05	0.032	0.052	3.67E + 05	3.60E + 05	1.65E + 05	2.22E + 05	0.0001	0.001
L5	3.89E + 04	4.71E + 04	2.68E + 04	3.99E + 04	0.094	0.119	4.22E + 04	5.14E + 04	1.90E + 04	3.23E + 04	0.002	0.006
L6	1.69E + 04	2.29E + 04	1.23E + 04	1.93E + 04	0.188	0.218	1.84E + 04	2.48E + 04	7881.95	1.47E + 04	0.003	0.007
L7	2.27E + 04	3.00E + 04	1.67E + 04	2.57E + 04	0.192	0.218	2.55E + 04	3.33E + 04	1.07E + 04	2.02E + 04	0.002	0.006
L8	1.45E + 04	1.77E + 04	1.13E + 04	1.41E + 04	0.23	0.254	1.52E + 04	1.79E + 04	7748.51	9940.33	0.003	0.007
L9	1.54E + 05	1.49E + 05	1.05E + 05	1.35E + 05	0.04	0.06	1.70E + 05	1.71E + 05	7.88E + 04	1.11E + 05	0.0003	0.002
GLGM												
MGR	5.38	5.13	15.01	30.35	0.004	0.015	6.84	11.92	16.39	30.79	0.008	0.013
VGR	6075.07	1657.75	2.33E + 05	8.91E + 05	0.02	0.037	4.19E + 04	2.48E + 05	2.92E + 05	9.06E + 05	0.015	0.021
Skewness	35.54	21.57	28.13	21.81	0.025	0.046	37.78	23.62	30.68	23.71	0.049	0.063
Kurtosis	1861.58	1757.05	1363.91	1621.03	0.054	0.073	2139.65	2239.33	1611.04	1982.97	0.101	0.115

* In right condyle analysis, 26 and 28 patients contributed 69 and 78 measurements to normal bone density and osteoporosis groups, respectively. In left condyle analysis, 24 patients contributed 68 and 69 measurements to normal bone density and osteoporosis groups, respectively. For all other analyses 29 patients contributed 87 measurements.

of the CT images [29]. Also, in the former study, apparent trabecular bone fraction and fractal dimension can use the combination to the BMD to provide better assessment of the fracture risk than that obtainable solely by BMD measurement [30]. According to our results, the osteoporotic bone has higher SRE, LRE, GLN, and RLN values, but has lower mean, median, RP, LGRE, HGRE, SRLGRE values compared to normal bone. This suggest that during the process of loss of BMD and progression towards osteoporosis, a larger amount of short line structures and a fewer amount of long line like structures, as evidenced by the lack of statistically significant differences in the LRLGE and LRHGE texture features. Comparing to the prior study, RLN can be different on the regions. Our results suggest that quantitative analysis of the microarchitecture in the cancellous bone on noncontrast head CT images can be used as a new indicator to diagnose osteoporosis.

As described above, osteoporosis is characterized by decrease in bone mass and alterations in bone tissue, resulting in increased bone fragility and an increased risk of fracture [2]. Part of the utility and strength of texture analysis lies in its ability to utilize structures included in studies performed for other clinical reasons as a screening modality to detect undetected osteoporosis in unscreened individuals. Data provided with head CT examinations may be used to identify patients with osteoporosis who are possibly at an increased risk for fracture without additional examinations, patient time, cost, and radiation.

This study has several limitations. First, there is a maximum one-year interval between head CT and DXA, which may have resulted in differences in BMD between the two studies. Second, only trabecular bone was included in the texture analysis obtained from CT, while DXA

assesses both cancellous and cortical bone. Although trabecular bone architecture parameters could add significant information beyond BMD for predicting bone strength, [23,25,26,31–34] this difference in bone types may have resulted in errors in the correlation between DXA the BMD and the texture parameters. In this preliminary investigation we did not account for possible medications which would alter BMD. Third, small sample size, the lack of hormonal data and the cause of osteoporosis have not been taken into account, as well as the absence of pathological radiographic correlation. This may be the focus of future a future investigation.

5. Conclusions

The results of this pilot study suggest that a texture analysis applied to noncontrast head CT may be helpful in identifying patients with osteoporosis. We are not suggesting that this modality and methodology replace conventional BMD screening tests, but rather this may be used to assess patients with limited access to conventional screening modalities and who may have already had a head CT performed for other routine clinical purposes. Despite the reduction in time associated with undergoing additional examinations, additional patient time, cost, and radiation exposure, this method may potentially help to decrease the total number of unscreened patients and untreated patients with osteoporosis.

Conflicts of interest and source of funding

None.

Funding sources

This research did not receive any specific grant from funding agencies in the public, commercial, or not-for-profit sectors

Transparency document

The Transparency document associated with this article can be found in the online version.

References

[1] X. Ouyang, S. Majumdar, T.M. Link, et al., Morphometric texture analysis of spinal trabecular bone structure assessed using orthogonal radiographic projections, Med. Phys. 25 (1998) 2037–2045, https://doi.org/10.1118/1.598391.
[2] F. Cosman, S.J. de Beur, M.S. LeBoff, et al., Clinician's guide to prevention and treatment of osteoporosis, Osteoporos. Int. 10 (2014) 2359–2381, https://doi.org/10.1007/s00198-015-3037-x.
[3] N.E. Lane, Epidemiology, etiology, and diagnosis of osteoporosis, Am. J. Obstet. Gynecol. 194 (2006) S3–S11, https://doi.org/10.1016/j.ajog.2005.08.047.
[4] T. Baum, M. Gräbeldinger, C. Räth, et al., Trabecular bone structure analysis of the spine using clinical MDCT: can it predict vertebral bone strength? J. Bone Miner. Metab. 32 (2014) 56–64, https://doi.org/10.1007/s00774-013-0465-6.
[5] N.C. Wright, A.C. Looker, K.G. Saag, et al., The recent prevalence of osteoporosis and low bone mass in the United States based on bone mineral density at the femoral neck or lumbar spine, J. Bone Miner. Res. 29 (2014) 2520–2526, https://doi.org/10.1002/jbmr.2269.
[6] H.D. Nelson, E.M. Haney, T. Dana, et al., Screening for osteoporosis: an update for the U.S. Preventive services task force, Ann. Intern. Med. 153 (2010) 99–111, https://doi.org/10.7326/0003-4819-153-2-201007200-00262.
[7] A.L. Amarnath, P. Franks, J.A. Robbins, et al., Underuse and overuse of osteoporosis screening in a regional health system: a retrospective cohort study, J. Gen. Intern. Med. 30 (2015) 1733–1740, https://doi.org/10.1007/s11606-015-3349-8.
[8] R.G. Miller, B.H. Ashar, J. Cohen, et al., Disparities in osteoporosis screening between at-risk African-American and white women, J. Gen. Intern. Med. 20 (2005) 847–851, https://doi.org/10.1111/j.1525-1497.2005.0157.x.
[9] I. Hamrick, Q. Cao, D. Agbafe-Mosley, et al., Osteoporosis healthcare disparities in postmenopausal women, J. Womens Health (Larchmt). 21 (2012) 1232–1236, https://doi.org/10.1089/jwh.2012.3812.
[10] T.M. Link, Osteoporosis imaging: state of the art and advanced imaging, Radiology 263 (2012) 3–17, https://doi.org/10.1148/radiol.12110462.
[11] M.S. Kavitha, S.Y. An, C.H. An, et al., Texture analysis of mandibular cortical bone on digital dental panoramic radiographs for the diagnosis of osteoporosis in Korean women, Oral Surg. Oral Med. Oral Pathol. Oral Radiol. 119 (2014) 346–356, https://doi.org/10.1016/j.oooo.2014.11.009.
[12] J.S. Bauer, T.M. Link, Advances in osteoporosis imaging, Eur. J. Radiol. 71 (2009) 440–449, https://doi.org/10.1016/j.ejrad.2008.04.064.
[13] M. Ito, Recent progress in bone imaging for osteoporosis research, J. Bone Miner. Metab. 29 (2011) 131–140, https://doi.org/10.1007/s00774-010-0258-0.
[14] R. Haralick, K. Shanmugam, I. Dinstein, Textural features for image classification, IEEE Trans. Syst. Man Cybern. A. Syst. Hum. 6 (1973) 610–621, https://doi.org/10.1109/TSMC.1973.4309314.
[15] K. Buch, A. Fujita, B. Li, et al., Using texture analysis to determine human papillomavirus status of oropharyngeal squamous cell carcinomas on CT, Am. J. Neuroradiol. 36 (2015) 1343–1348, https://doi.org/10.3174/ajnr.A4285.
[16] M. de Carvalho Alegro, A. Valotta Silva, S. Yumi Bando, et al., Texture analysis of high resolution MRI allows discrimination between febrile and afebrile initial precipitating injury in mesial temporal sclerosis, Magn. Reson. Med. 68 (2012) 1647–1653, https://doi.org/10.1002/mrm.24174.
[17] M.E. Mayerhoefer, D. Stelzeneder, W. Bachbauer, et al., Quantitative analysis of lumbar intervertebral disc abnormalities at 3.0 Tesla: value of T_2 texture features and geometric parameters, NMR Biomed. 5 (2012) 866–872, https://doi.org/10.1002/nbm.1803.
[18] F. Risse, J. Pesic, S. Young, et al., A texture analysis approach to quantify ventilation changes in hyperpolarised ^{3}He MRI of the rat lung in an asthma model, NMR Biomed. 25 (2012) 131–141, https://doi.org/10.1002/nbm.1725.
[19] K. Fujimoto, T. Tonan, S. Azuma, et al., Evaluation of the mean and entropy of apparent diffusion coefficient values in chronic hepatitis C: correlation with pathologic fibrosis stage and inflammatory activity grade, Radiology 258 (2011) 739–748, https://doi.org/10.1148/radiol.10100853.
[20] D. Jirák, M. Dezortová, P. Taimr, et al., Texture analysis of human liver, J. Magn. Reson. Imaging 15 (2002) 68–74, https://doi.org/10.1002/jmri.10042.
[21] B. Barry, K. Buch, J.A. Soto, et al., Quantifying liver fibrosis through the application of texture analysis to diffusion weighted imaging, Magn. Reson. Imaging 32 (2014) 84–90, https://doi.org/10.1016/j.mri.2013.04.006.
[22] J.A. Kanis, L.J. Melton 3rd, C. Christiansen, et al., The diagnosis of osteoporosis, J. Bone Miner. Res. 9 (1994) 1137–1141, https://doi.org/10.1002/jbmr.5650090802.
[23] M. Hudelmaier, A. Kollstedt, E.M. Lochmüller, et al., Gender differences in trabecular bone architecture of the distal radius assessed with magnetic resonance imaging and implications for mechanical competence, Osteoporos. Int. 16 (2005) 1124–1133, https://doi.org/10.1007/s00198-004-1823-y.
[24] K.I. Laws, Textured Image Segmentation, No. USCIPI-940 University of Southern California Los Angeles Image Processing INST, 1980.
[25] T.M. Link, S. Majumdar, J.C. Lin, et al., Assessment of trabecular structure using high resolution CT images and texture analysis, J. Comput. Assist. Tomogr. 22 (1998) 15–24, https://doi.org/10.1097/00004728-199801000-00003.
[26] T.M. Link, S. Majumdar, J.C. Lin, et al., A comparative study of trabecular bone properties in the spine and femur using high resolution MRI and CT, J. Bone Miner. Res. 13 (1998) 122–132, https://doi.org/10.1359/jbmr.1998.13.1.122.
[27] M.E. Glickman, S.R. Rao, M.R. Schultz, False discovery rate control is a recommended alternative to Bonferroni-type adjustments in health studies, J. Clin. Epidemiol. 67 (2014) 850–857, https://doi.org/10.1016/j.jclinepi.2014.03.012.
[28] M. Ito, M. Ohki, K. Hayashi, et al., Trabecular texture analysis of CT images in the relationship with spinal fracture, Radiology 194 (1995) 55–59, https://doi.org/10.1148/radiology.194.1.7997582.
[29] N.P. Castellanos, E. Martínez, J. Gutierrez, Improving osteoporosis diagnosis in children using image texture analysis, Conf. Proc. IEEE Eng. Med. Biol. Soc. 2011 (2011) 6184–6187, https://doi.org/10.1109/IEMBS.2011.6091527.
[30] E. Lespessailles, C. Gadois, I. Kousignian, et al., Clinical interest of bone texture analysis in osteoporosis: a case control multicenter study, Osteoporos. Int. 7 (2008) 1019–1028, https://doi.org/10.1007/s00198-007-0532-8.
[31] S.L. Greenspan, S. Perera, R. Recker, et al., Changes in trabecular microarchitecture in postmenopausal women on bisphosphonate therapy, Bone 46 (2010) 1006–1010, https://doi.org/10.1016/j.bone.2009.12.025.
[32] J.S. Bauer, S. Kohlmann, F. Eckstein, et al., Structural analysis of trabecular bone of the proximal femur using multislice computed tomography: a comparison with dual X-ray absorptiometry for predicting biomechanical strength in vitro, Calcif. Tissue Int. 78 (2006) 78–89, https://doi.org/10.1007/s00223-005-0070-3.
[33] T. Baum, J. Carballido-Gamio, M.B. Huber, et al., Automated 3D trabecular bone structure analysis of the proximal femur-prediction of biomechanical strength by CT and DXA, Osteoporos. Int. 21 (2010) 1553–1564, https://doi.org/10.1007/s00198-009-1090-z.
[34] T. Baum, M. Kutscher, D. Müller, et al., Cortical and trabecular bone structure analysis at the distal radius-prediction of biomechanical strength by DXA and MRI, J. Bone Miner. Metab. 31 (2013) 212–221, https://doi.org/10.1007/s00774-012-0407-8.